

Research Article

A Decrease in NiO-MgO Phase Through Its Solid Solution Equilibrium with Tetragonal $(\text{La}_{1-z}\text{Sr}_z)_2\text{Ni}_{1-y}\text{Mg}_y\text{O}_{4-\delta}$: Effect on Catalytic Partial Oxidation of Methane

Xiong Yin,¹ Liang Hong,^{1,2} and Zhengliang Gong¹

¹ Department of Chemical and Biomolecular Engineering, National University of Singapore, BLK E5 02-02,

4 Engineering Drive 4, Singapore 117576

² Institute of Materials Research and Engineering, 3 Research Link, Singapore 117602

Correspondence should be addressed to Liang Hong, chehongl@nus.edu.sg

Received 2 March 2011; Accepted 11 June 2011

Academic Editor: Hahmid Reza Zargar

Copyright © 2012 Xiong Yin et al. This is an open access article distributed under the Creative Commons Attribution License, which permits unrestricted use, distribution, and reproduction in any medium, provided the original work is properly cited.

Calcination of an oxide mixture consisting of 0.4 La_2O_3 , 0.2 SrCO_3 , $(1-x)\text{NiO}$, and $x\text{MgO}$ at 800°C results in an equilibrium between tetragonal $(\text{La}_{1-z}\text{Sr}_z)_2\text{Ni}_{1-y}\text{Mg}_y\text{O}_{4-\delta}$ phase and NiO-MgO phase. Forming rock-salt NiO-MgO facilitates the NiO to join the tetragonal phase. The size of the NiO-MgO phase in the resulting composite is reduced with the increase in MgO (the x value). The composite thus obtained is used to catalyze partial oxidation of methane, and the maximum methane conversion of ca. 93% is achieved when $x = 0.2$. A further rise in x value results in a monotonic decrease in the methane conversion. X-ray diffraction, electron microscopy, and chemisorption all confirm a decrease in both size and amount of the supported Ni^0 clusters with the increase in MgO dosage. The reduction in size promotes the dispersion of Ni^0 sites and gives rise to both high activity and strong coking resistance.

1. Introduction

Reforming of natural gas (mainly CH_4) into syngas (a mixture of H_2 and CO) is an important industrial process. Syngas is the feedstock of hydrogen, synthetic liquid fuel with ultra-low sulfur, and other value-added chemicals [1–5]. In addition, it can also be used to power solid oxide fuel cells (SOFC). The techniques of transforming methane to syngas include steam reforming, CO_2 reforming and partial oxidation. Steam reforming ($\text{CH}_4 + \text{H}_2\text{O} \rightarrow \text{CO} + 3\text{H}_2$, $\Delta H_{298\text{K}}^0 = +206 \text{ kJ/mol}$) and CO_2 reforming ($\text{CH}_4 + \text{CO}_2 \rightarrow 2\text{CO} + 2\text{H}_2$, $\Delta H_{298\text{K}}^0 = +247 \text{ kJ/mol}$) are highly energy intensive reactions. The steam reforming of methane (SRM) has still been the primary commercial process of syngas production despite its high capital cost [6–10]. On the contrary, the partial oxidation of methane (POM), being mild exothermic in nature ($\text{CH}_4 + (1/2)\text{O}_2 \rightarrow \text{CO} + 2\text{H}_2$; $\Delta H_{298\text{K}}^0 = -36 \text{ kJ/mol}$), is attractive for the production of syngas. Nevertheless, a lack of POM catalyst with both acceptable cost to industry and long-term stable catalytic

performance is the major barrier to the commercialization of the POM process [11–13].

Supported Ni catalysts are very attractive for industrial application because of their low cost and high POM catalytic activity. Nevertheless, most of the Ni-based catalysts are vulnerable to carbon deposition over the metallic Ni particles. Thus, ameliorating chemical resistance of the supported-Ni catalysts against coking has become an area of intensive research since the publication of Prettre et al. [14]. In consequence, different approaches have been developed to date to tackle this problem. Amid them, amalgamation of alkali elements [15], alkaline earth elements [16, 17], or rare earth elements [18] with different types of supports has received positive impacts. Doping Ni surface with other metals to form a surface alloy was also found effective [19–21]. More recently, Ni-containing perovskite oxides were identified to be a unique type of catalytic system for POM. This finding is related to the in situ generation of very tiny metallic Ni nuclei under the POM reaction condition [22–28]. The other noticeable progress was the development

of a protective chemical environment for the Ni catalytic site in nanoscale. Ruckenstein and Hu found that MgO support can stabilize the nickel catalytic sites in the POM reaction due to the formation of a NiO in MgO solid solution [16]. Alternatively, Takenaka et al. [29] disclosed the water-in-oil microemulsion method for the preparation of nanosized nickel metal particles (5 nm) encapsulated by a 10 nm-thick silica shell. This thin shell was confirmed to enhance the POM catalytic stability of the Ni particles enclosed. More recently, Iriando et al. also proposed that interactions between Ni⁰ and MgO promoted the yield of H₂ in the product of steam reforming of glycerol [30].

To achieve nano-Ni metal particles that are embedded on the surface of an appropriate support, we have developed a K₂NiF₄-supported Ni⁰ catalyst that displays promising POM catalytic activity and stability. This outcome originates from preserving a small amount of NiO during the preparation of the precursor of catalyst, a double perovskite-type oxide (La_{0.5}Sr_{0.5})₂FeNiO_{6-δ} [31]. In this study, the concept is furthered through utilizing the solid state reaction equilibrium between the two solid solutions: the rock salt NiO-MgO and the tetragonal (La_{1-z}Sr_z)₂Ni_{1-y}Mg_yO_{4-δ} (LSNM). The latter one is the major phase in the oxide composite. This design came from the observation of the calcination of an oxide mixture of 0.4 La₂O₃, 0.2 SrCO₃, (1 - x)NiO and xMgO with the stoichiometry as indicated. The presence of a small amount of MgO changes the path of this solid state reaction. Namely, the reaction no longer produces orthorhombic and then perovskite structures with the increase in calcination temperature. Instead, the reaction produces a mixture comprising the tetragonal (La_{1-z}Sr_z)₂Ni_{1-y}Mg_yO_{4-δ} phase, the NiO-MgO solid solution phase, and residues of the other two oxides. With the increase in the stoichiometry of MgO from x = 0.1 to x = 0.5 in the feed, it is found that more NiO-MgO phase will be assimilated into the tetragonal phase at the same calcinations temperature. Hence, this phase transition allows realizing a low-volume fraction but highly dispersed NiO-MgO phase with dilute NiO in it at equilibrium. As a result, this leads to small sizes of Ni(0) clusters that are imbedded in the MgO phase after the mixture is subjected to the reducing atmosphere of POM. Through this synthetic route for Ni(0) clusters, the effect of MgO stoichiometry on the performance of the catalyst in POM was investigated from the fundamental perspective in this work.

2. Experimental

2.1. Preparation of Catalyst Precursors. An oxide mixture of 0.4 La₂O₃, 0.2 SrCO₃, (1 - x)NiO, and xMgO (x = 0, 0.1, 0.2, 0.3, 0.4, 0.5) were prepared by the Pechini method [31]. Stoichiometric amounts of metal (La, Sr, Mg, and Ni) nitrates were dissolved in deionized (DI) water, followed by the addition of citric acid and glycine. The mole ratio of total metal (La, Sr, Mg, and Ni) nitrates : citric acid : glycine was 2 : 1 : 1. The solution was then thickened at 80°C until a gel was formed. The gel was subjected to calcination at 400°C for 2 h, after which a fine powder was

produced. The powder was further calcined at 800°C for 1 h under ambient atmosphere to produce the catalyst precursor.

2.2. Partial Oxidation of Methane. POM was carried out in a fixed-bed microreactor under an atmospheric pressure. The catalyst precursor (100 mg) was loaded in a tubular quartz reactor (I.D. = 8 mm). With the purpose of running POM at isothermal condition, CH₄ and air was mixed with an excess of He to form the feed stream with the volume ratio of CH₄:O₂:N₂:He = 2:1:4:38. Although a low concentration of CH₄ in the feed stream was used, a very high hourly space velocity (GHSV) of 45,780 cm³/(g-h) at STP, which is equivalent to 2,035 cm³/g-h of pure methane, was set to operate the POM. The reaction temperature was set at 850°C in this work, since it is known as the upper middle temperature for POM. The compositions of the reactant and product streams were analyzed by gas chromatography (Perkin Elmer ARNEL, Clarus 500) equipped with TCD detector. The methane conversion (X_{CH₄}), CO selectivity (S_{CO}), and H₂ selectivity (S_{H₂}) were calculated by the following formulae:

$$\begin{aligned} X_{\text{CH}_4} &= \frac{[\text{CH}_{4,\text{in}}] - [\text{CH}_{4,\text{out}}]}{[\text{CH}_{4,\text{in}}]} \times 100\% \\ S_{\text{CO}} &= \frac{[\text{CO}_{\text{out}}]}{[\text{CH}_{4,\text{in}}] - [\text{CH}_{4,\text{out}}]} \times 100\% \\ S_{\text{H}_2} &= \frac{0.5 \times [\text{H}_{2,\text{out}}]}{[\text{CH}_{4,\text{in}}] - [\text{CH}_{4,\text{out}}]} \times 100\%. \end{aligned} \quad (1)$$

2.3. Characterization of Catalysts. Crystalline structures of the catalyst precursor formed after being calcined at 800°C and used subsequently in a POM run at 850°C were determined by X-ray diffraction (XRD, SHIMADZU XRD-6000, and Cu K α radiation) using a scanning rate of 2°/min. The micromorphologies of the catalyst precursors were scrutinized on a field emission scanning electron microscope (FESEM, JEOL JSM-6700F). The images of the nanoscaled Ni clusters were obtained from a transmission electron microscope (TEM, JEOL JEM-2100F). Investigation of the surface state of oxygen species was conducted on an X-ray photoelectron spectrometer (Kratos AXIS HSi System XPS) equipped with Al K α X-ray source (1486.6 eV) and the take-off angle of 90° with pass energy of 40 eV. C1s (284.6 eV) was used as the internal reference for this characterization.

The adsorption/desorption isotherm of N₂, the temperature-programmed reduction with H₂ (H₂-TPR) and the temperature-programmed desorption with He (O₂-TPD) were performed on a physicochemical adsorber (Quantachrome Autosorb-1 instrument). The specific surface area of a sample was determined by applying the multipoint BET method. The pore volume and average pore diameter of catalyst precursors were obtained from the N₂ desorption isotherm using the BJH method. The H₂-TPR was performed using a sample of 50 mg and a gas (5% H₂ in N₂) flow rate of 80 mL min⁻¹. The O₂-TPD was performed using a sample of 200 mg and a He flow rate of 80 mL min⁻¹. The heating rate

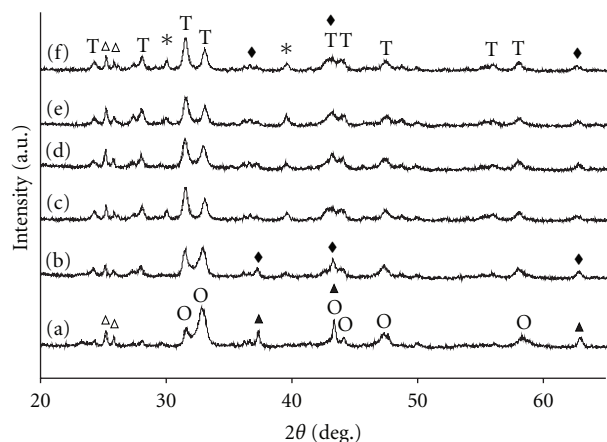


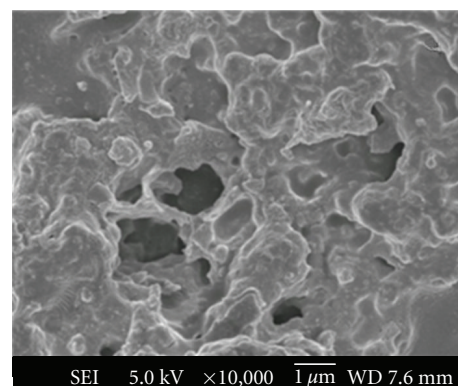
FIGURE 1: X-ray diffraction (XRD) patterns of the catalyst precursors made of $0.4 \text{ La}_2\text{O}_3-0.2 \text{ SrO}-(1-x)\text{NiO}-x\text{MgO}$ ($^{\text{T}}$ tetragonal $(\text{La}_{1-z}\text{Sr}_z)_2\text{Ni}_{1-y}\text{Mg}_y\text{O}_{4-\delta}$, $^{\text{O}}$ orthorhombic $(\text{La}_{1-z}\text{Sr}_z)_2\text{NiO}_{4-\delta}$, $^{\Delta}$ La_2O_3 , $^{\triangle}$ SrCO_3 , $^{\blacklozenge}$ NiO/MgO solution, $^{\blacktriangle}$ NiO): (a) $x = 0$, (b) $x = 0.1$, (c) $x = 0.2$, (d) $x = 0.3$, (e) $x = 0.4$, (f) $x = 0.5$.

for both TPR and TPD was set as $15^\circ\text{C}/\text{min}$ below 850°C and $1^\circ\text{C}/\text{min}$ above 850°C .

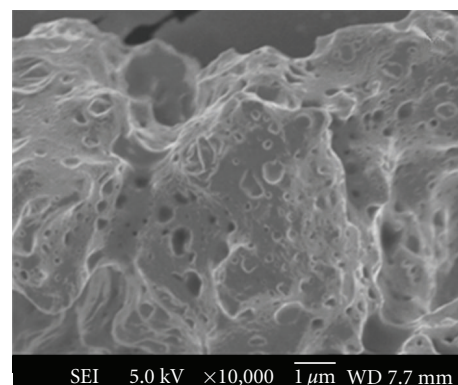
3. Results and Discussion

3.1. Impacts of MgO on the Solid State Reaction Equilibrium.

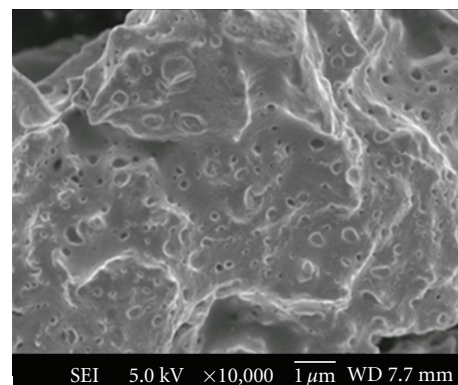
When a mixture of the metal oxides generated from metallo-organic gel (Section 2.1) is subjected to calcination, solid state reaction among the oxides takes place. The reaction extent and the composition of product depend on both the identities of the oxides and the calcination temperature. When the tricomponent mixture of $0.4 \text{ La}_2\text{O}_3$, 0.2 SrCO_3 , and NiO is subjected to calcination, an orthorhombic structure $(\text{La}_{1-z}\text{Sr}_z)_2\text{NiO}_{4-\delta}$ (LSN) is generated at 800°C , and then, a pure perovskite solid solution is resulted at 900°C [32]. However, introduction of a small amount of MgO into the above trioxide mixture, for instance, $0.4 \text{ La}_2\text{O}_3$, 0.2 SrCO_3 , 0.9 NiO , and 0.1 MgO , a tetragonal phase $(\text{La}_{1-z}\text{Sr}_z)_2\text{Ni}_{1-y}\text{Mg}_y\text{O}_{4-\delta}$ (LSNM) becomes predominant (Figure 1) in the resultant composite after calcination at 800°C . A rise of the NiO/MgO stoichiometry ratio in the 4-oxide feed to 8:2, the tetragonal phase becomes solely present. Besides the tetragonal phase, the La_2O_3 , SrCO_3 , and NiO-MgO solid solutions are also found in the XRD diagram. Moreover, with the increase in MgO in the feed, the NiO-MgO phase in the composite decreases. This trend can be discerned from the reduction in intensity of the peaks at 37.5° and 63° as the other peaks of the NiO-MgO phase overlap with those of the tetragonal phase. Accompanying this change, more tetragonal phase was formed in accordance with the rise of its main XRD peak areas (e.g., $2\theta = 31.5^\circ$ and 33°). The other role of MgO is to impede the generation of perovskite structure even when the calcination temperature was raised beyond 900°C . Moreover, accompanying the increase of MgO in the feed, the composite resulted from the solid state reaction at 800°C becomes slightly more porous (Figure 2). However, the BET surface area analysis shows just



(a)



(b)



(c)

FIGURE 2: The FESEM images of the catalyst precursors made of $0.4 \text{ La}_2\text{O}_3-0.2 \text{ SrO}-(1-x)\text{NiO}-x\text{MgO}$: (a) $x = 0$ (b) $x = 0.1$ and (c) $x = 0.5$.

little difference in the pore volumes and pore diameters amid the six samples, while the MgO content promotes the BET surface area of the samples to a finite extent (Table 1).

In light of the H_2 -TPR analysis of the six samples of the composite, according to their XRD identifications, only the orthorhombic LSN and NiO or tetragonal LSNM and the NiO-MgO phases can be reduced under the condition of analysis. Each sample shows three characteristic peaks on its TPR diagram (Figure 3). The peak at the temperature around 400°C (peak I) is ascribed to the reduction of Ni^{3+}

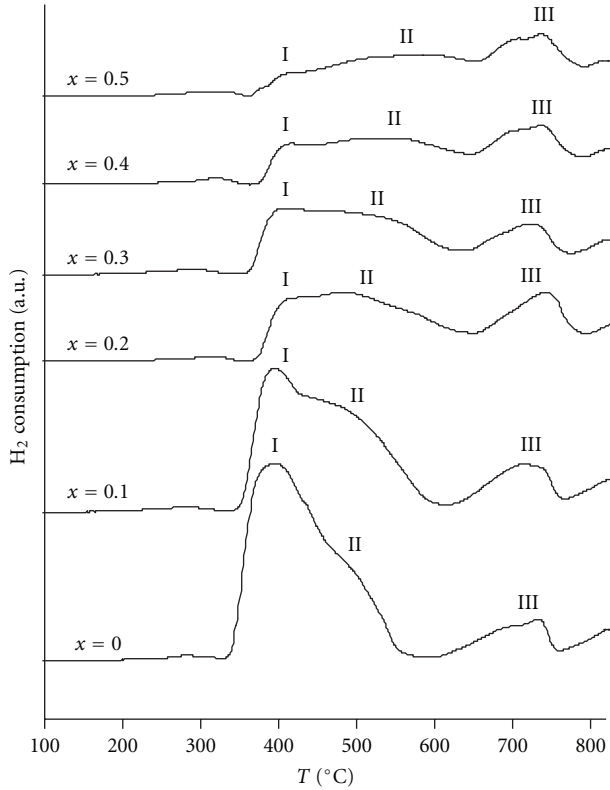


FIGURE 3: H_2 -TPR curves of the catalyst precursors made of $0.4 La_2O_3-0.2 SrO-(1-x)NiO-xMgO$.

TABLE 1: Surface area, pore volume, and pore diameter of the solid reaction products from the oxide mixtures: $0.4 La_2O_3-0.2 SrO-(1-x)NiO-xMgO$.

Parameters*	$x = 0$	$x = 0.1$	$x = 0.2$	$x = 0.3$	$x = 0.4$	$x = 0.5$
S_{BET} (m^2/g)	8	9	10	12	14	17
V_p (cm^3/g)	0.07	0.09	0.09	0.09	0.13	0.09
D_{ave} (nm)	35	37	38	32	37	22

*The multipoint BET surface area (S_{BET}), BJH desorption pore volume (V_p), and the average pore diameter (D_{ave}) of the prepared catalyst precursors.

ions in the orthorhombic ($x = 0$) or in tetragonal phase to Ni^{2+} [27, 33]. It is important to note that this peak becomes weaker with the increase in Mg^{2+} doping extent. Peak II arising in the temperature range from $500^\circ C$ to $600^\circ C$ is due to the reduction of NiO, which is alone when $x = 0$ but mixed with MgO when $x > 0$, to form metallic Ni^0 . Peak III at the temperature higher than $700^\circ C$ is related to the reduction of a part of Ni^{2+}/Ni^{3+} ions in above LSN and LSNM solid solutions into metallic Ni^0 [34]. Thus, the last TPR peaks have basically similar peak areas except the first TPR diagram. The first diagram exhibits the strongest first reduction peak and the smallest last peak amid the six. It implies that a significant part of Ni^{3+} ions in the orthorhombic phase has been directly reduced to Ni^0 in the lower temperature range as proposed above. The decrease in peak I with increasing of the x value is an indication

of the drop of reducibility of Ni^{3+} ions with more MgO being assimilated in the tetragonal phase. It is noteworthy that peak II also becomes weaker and shifts toward high temperature side also with the increasing of MgO. This variation is in agreement with the XRD results as exhibited in Figure 1, which shows that the NiO-MgO solid solution diminishes with increasing of the MgO component. The rise of reduction temperature implies the NiO is better protected by MgO because of more MgO present in the solid solution. It is a clear message for the change of chemical environment of Ni^0 metal clusters generated through the reduction in the NiO domains. In this context, the higher the TPR temperature will be the smaller and the better protected Ni^0 clusters will be produced, and hence, the less reactive they are. As a result, an optimal tradeoff between reactivity and stability of Ni^0 clusters exists, which will be found when the resulting catalysts are assessed in POM. Furthermore, TRP peak III also signifies the degradation of the orthorhombic phase or a part of the tetragonal phase to La-Sr-O oxide, in which the Ni^0 clusters produced were to be imbedded in situ. This point will be further elaborated in the following evaluation of POM. Furthermore, we also examined the six samples downloaded from TPR measurement by TEM. Three samples (with $x = 0, 0.1$ and 0.5) were selected to check the generation of Ni^0 phase (Figure 4). Indeed, it can be seen that the Ni^0 clusters formed in the La-Sr-O oxide and in the MgO oxide decrease in number and size with the increase in MgO content. Typically, the heavy presence of Ni^0 particles in the first sample verifies the strongest first TPR peak this sample exhibits, which has been ascribed to the reduction of Ni^{3+} to Ni^0 , since its third TPR peak is the weakest among the six samples.

3.2. The Oxygen Desorption of the Catalyst Precursors . TPD diagrams of the six samples all exhibit two oxygen desorption peaks (Figure 5). As to the first peak, which appears in the temperature range from $360^\circ C$ to $440^\circ C$, its apex moves toward a higher temperature with the increase in MgO in the 4-oxide feed, $0.4 La_2O_3-0.2 SrO-(1-x)NiO-xMgO$. This desorption peak has been ascribed to the oxygen molecules adsorbed at surface oxygen vacancies (α oxygen) [35–37]. Likewise, an apparent increase in the peak area is also observed with the increase in the x value, meaning that more molecular oxygen desorbs. The above discussion has concluded that the B-site composition, $Ni_{1-y}Mg_y$, in the tetragonal LSNM has a higher y stoichiometric coefficient with the increase in the x value in the feed. This divalent-ion doping is to cause a higher concentration of oxygen vacancies in the LSNM phase, that is, δ . As a result, the concentration of molecular oxygen adsorbed at the surface vacancies including nonstoichiometric oxygen increases, or the oxygen storage capability mounts. Correspondingly, with the increasing of the y value, the adsorbed molecular oxygen requires higher temperature to leave the adsorbent. Regarding the desorption peak arising in temperature range from $600^\circ C$ to $800^\circ C$, it is attributed to the desorption of lattice oxygen (O^{2-} , β oxygen) [36–38]. This desorption occurs accompanying the reduction of a certain number

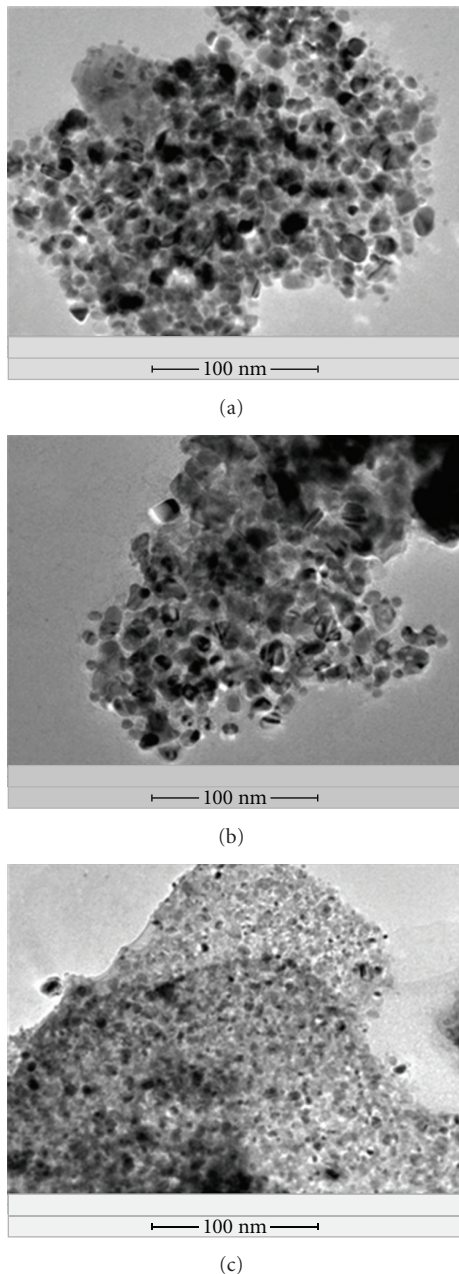


FIGURE 4: TEM images of the H_2 -reduced catalyst precursors made of $0.4 La_2O_3-0.2 SrO-(1-x) NiO-xMgO$: (a) $x = 0$, (b) $x = 0.1$, (c) $x = 0.5$, in which the dark micro-domains are embedded Ni^0 clusters.

of Ni^{3+} ions to Ni^{2+} ions in order to balance the positive charge generated. It is worthy of note that the MgO content (the x value) in the solid reaction mixture affects the extent of desorption and desorption temperature as well. When $x = 0$, this TPD peak was substantially weak, but it turns to much stronger and shifted to a higher temperature with the increase in the x value to 0.1. After that, the peak area increases gradually with the increase in the content of MgO. It is expected that substitution of Mg^{2+} for Ni^{3+} in the B-site of LSM would enhance the ionic bonding

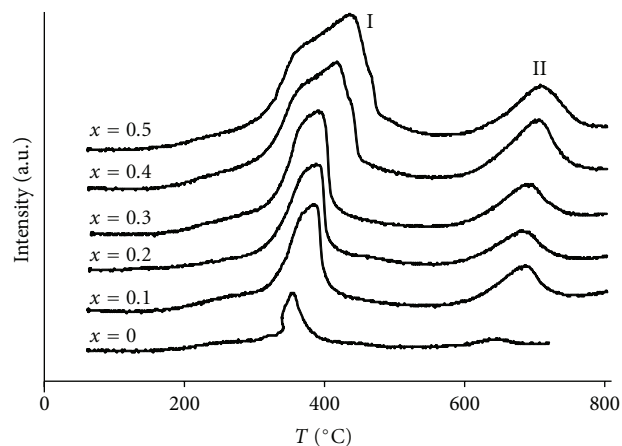


FIGURE 5: O_2 -TPD curves of the catalyst precursors made of $0.4 La_2O_3-0.2 SrO-(1-x) NiO-xMgO$.

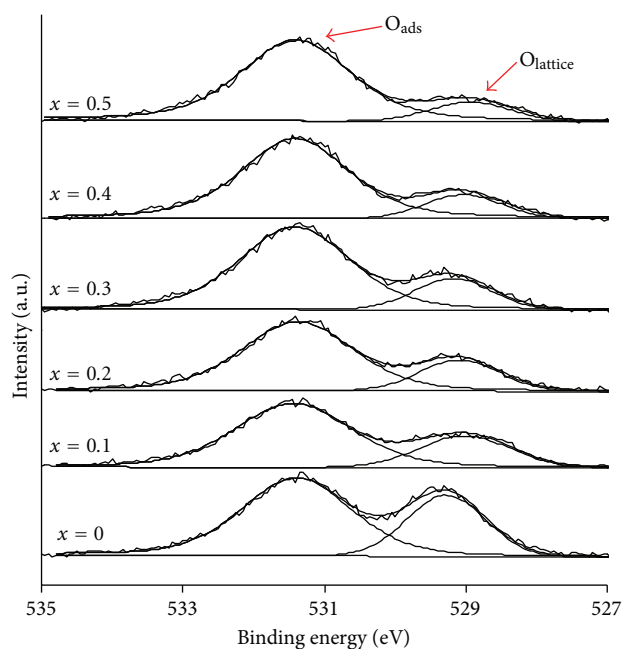


FIGURE 6: $O1s$ XPS of the catalyst precursors made of $0.4 La_2O_3-0.2 SrO-(1-x) NiO-xMgO$.

nature, which can be proved by the increase of the charge on the lattice O^{2-} ions by $O1s$ XPS, and hence promote the mobility of lattice oxygen. At the same time, with the increase in the concentration of lattice oxygen vacancy, the desorption temperature increases, implying the restriction to the desorption of lattice oxygen. From the TPD result, the restriction factor can be overcome at a relatively higher temperature.

The chemical environments of oxygen species in the composite were also investigated by XPS. All the six samples exhibit two peaks at 529.5 eV and 531.5 eV in the $O1s$ spectrum (Figure 6). The former peak has been ascribed to the lattice O^{2-} ($O_{lattice}$) while the latter one to the surface adsorbed oxygen species (O_{ads}) such as $-OH$ [39]. The

TABLE 2: XPS ratios of $O_{\text{lattice}}/O_{\text{ads}}$ species in the different catalysts made of the oxide mixtures $0.4 \text{ La}_2\text{O}_3-0.2 \text{ SrO}-(1-x)\text{NiO}-x\text{MgO}$.

Different stoichiometry coefficient x	XPS ratios of $O_{\text{lattice}}/O_{\text{ads}}$ species
$x = 0$	0.55
$x = 0.1$	0.36
$x = 0.2$	0.27
$x = 0.3$	0.23
$x = 0.4$	0.18
$x = 0.5$	0.15

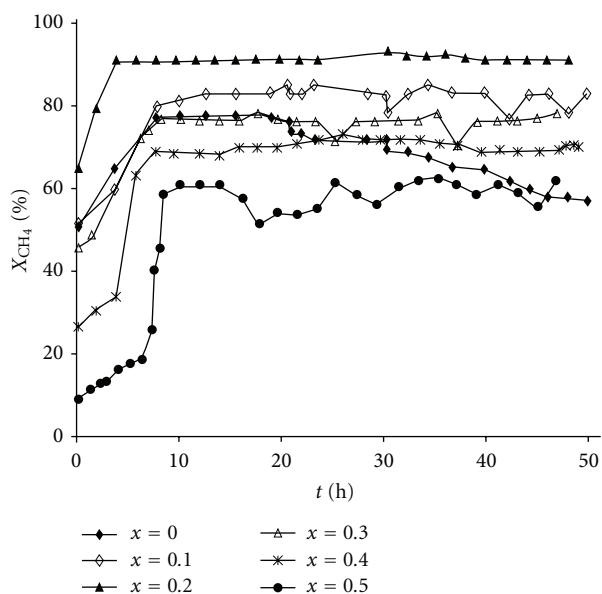
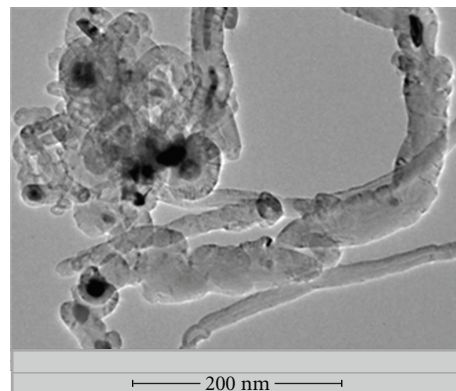


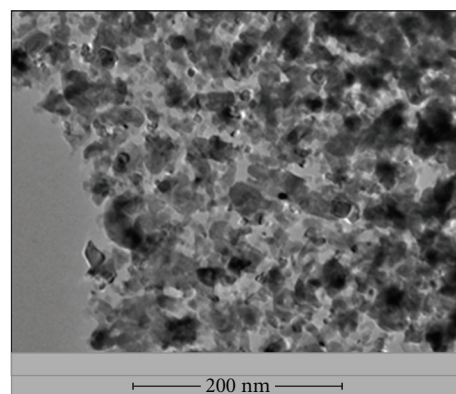
FIGURE 7: POM evaluation of the catalysts generated in situ from the precursors made of $0.4 \text{ La}_2\text{O}_3-0.2 \text{ SrO}-(1-x)\text{NiO}-x\text{MgO}$ at 850°C over a duration of 50 h.

peak area ratio ($O_{\text{lattice}}/O_{\text{ads}}$) represents the atomic ratio of lattice oxygen to oxygen vacancies at surface. The numerical values of the ratio are summarized in Table 2. Clearly, the ratio decreases as the increase in the MgO dosage. It is, therefore, suggested that the concentration of the adsorbed oxygen species be promoted by the oxygen vacancies in the tetragonal LSNM. In addition, we also notice that the binding energy of the lattice O^{2-} slightly reduces with the increase in the Mg^{2+} doping (the x value). It could be interpreted as the promotion of ionic character of the lattice oxygen due to the induction effect of Mg^{2+} ions, which makes the lattice oxygen more mobile because of the decrease in the covalent component.

3.3. Effects of Active Ni^0 Cluster Sizes and Their Exposure on POM. In the context of the above discussion, the Ni^0 clusters generated from the reduction (the TPR experiment) locate in two types of microenvironments: in the La-Sr-O oxide and MgO degraded from the tetragonal phase and in MgO derived from the NiO-MgO solid solution. Additionally,



(a)



(b)

FIGURE 8: TEM examination of the two representative used catalysts after 50 h POM at 850°C (with reference to Figure 7): (a) $x = 0$, (b) $x = 0.2$.

accompanying the increase in MgO, the Ni^0 clusters become smaller in these two locations. Under the POM condition, the nickel ions in each sample loaded are to undergo the reduction similarly by methane to form Ni^0 clusters, namely, in situ generation of the catalytic sites.

After the six samples (or precursors) were loaded respectively in a fixed-bed microreactor, it took about 8 hours to fully convert them to the desired catalysts (i.e., activation) under the reaction condition (Figure 7). Then, the evaluation of their POM reactivity was carried out over a reaction course of 50 h at 850°C . We selected a low- CH_4 feed stream but a high GHSV to evaluate the catalyst. This arrangement could be more sensitive to reflect any loss of catalytic activity than the use of a higher concentration but low space velocity, since methane has a shorter residential time in our setting. The catalyst with nil MgO could retain a CH_4 conversion rate of 78% for around 12 h before declining. At the end of the reaction, the conversion dropped to 58%, and this loss of activity is attributed to the formation of a large extent of carbon filaments on the metallic Ni^0 surface (Figure 8(a)). Besides susceptibility to coking, this catalyst has the highest Ni content, but the Ni^0 sites were apparently not fully used. Such a performance can be traced to the large Ni^0 particles present in the catalyst as shown in Figure 4(a),

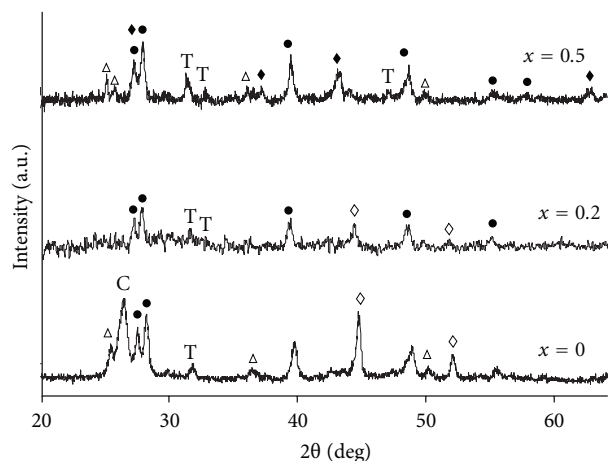


FIGURE 9: XRD patterns of the three used catalysts after POM for 50 h at 850°C (with reference to Figure 7): T the tetragonal phase, \bullet La-Sr-O, \triangle SrCO₃, \blacklozenge NiO/MgO solution, \diamond Ni⁰, and C carbon.

namely, presenting a poor Ni⁰ dispersibility. In contrast to this, the incorporation of a small amount of MgO ($x = 0.1$ and 0.2) into this catalyst system brought about tangible improvement on the catalytic activity. The catalyst with $x = 0.2$ displayed the best performance indicated by conversion and stability. None of carbon filaments were found on the catalyst downloaded from the reactor (Figure 8(b)). A scrutinizing of the TEM images can find that carbon filament grows from Ni⁰ particles of about 20 nm Figure 8(a), while the Ni⁰ particles in Figure 8(b) are smaller, and many of them are surrounded or partially surrounded by a layer, supposedly to be the mixture of La-Sr-O and MgO as proposed above. Alternatively, the catalysts with higher MgO doping extents ($x > 0.2$) resulted in monotonic reduction in the conversion rate. It has been aware of the roles of MgO from the above elaboration: facilitating entering of NiO into the tetragonal phase, suppressing reducibility of the tetragonal phase, and reducing the amount of NiO/MgO solid solution as well as the NiO content in it. Hence, the reactivity declining is not unexpected because of the reduction in both the number and exposure of Ni⁰ clusters, which has been unveiled in Figure 4(c). In addition, XRD patterns of the three catalysts ($x = 0, 0.2$ and 0.5) after POM of 50 h were collected (Figure 9) for further examination. The Ni⁰ cluster peak arising in the three diffraction patterns became weaker with the increase in x value. It is, thereby, confirmed that the catalyst with MgO doping level at $x = 0.2$ balanced the need of both activity and coke resistance. In the meantime, only the XRD pattern ($x = 0$) displayed strong carbon peak, indicating its heavy coking extent, which is plausible to the preceding TEM observation. In addition, the figure also shows that the catalyst with the highest MgO doping ($x = 0.5$) could retain to the highest extent the tetragonal phase. This evidence supports the decreasing of the reducibility of the tetragonal phase with the increasing of MgO doping observed from the TPR analysis.

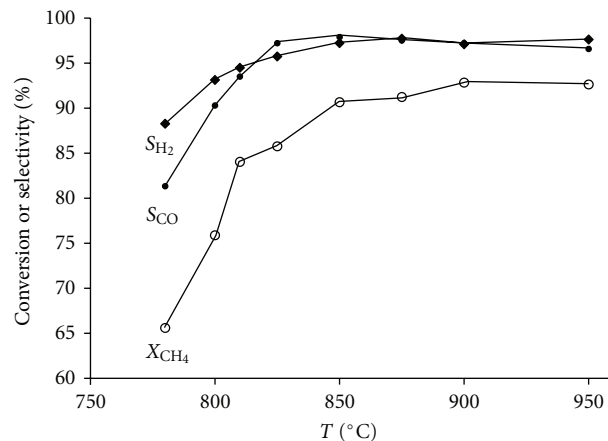


FIGURE 10: Evaluation of temperature effect on the methane conversion and selectivity to H₂ and CO in the POM sustained by the catalyst with $x = 0.2$.

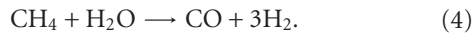
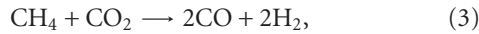
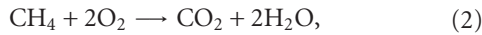
TABLE 3: Coke deposited on the catalysts generated from the oxide mixtures: 0.4 La₂O₃-0.2 SrO-(1- x)NiO- x MgO after POM at 850°C over 50 h.

Different stoichiometry coefficient x	Coke on catalyst (wt%)
$x = 0$	20.7
$x = 0.1$	4.5
$x = 0.2$	1.6
$x = 0.3$	1.3
$x = 0.4$	0.8
$x = 0.5$	0.3

After clarifying the influence due to the presence of MgO in the catalyst precursor on the POM catalytic activity, we then looked at the effect of reaction temperature by using the catalyst precursor with $x = 0.2$ as the model system. The precursor was first subjected to activation for 10 h at 900°C in the microreactor before checking the composition of outlet stream. At each testing temperature, a three-hour dwelling period was set before collecting the experimental data. The catalyst was very stable at each testing temperature, whose performance data are summarized in Figure 10. The methane conversion (X_{CH_4}) levelling off at 900°C claimed the maximum reading of ca. 93% while both CO selectivity (S_{CO}) and H₂ selectivity (S_{H_2}) reached ca. 97% at a lower temperature of ca. 840°C. This phenomenon suggests that the catalyst have more powerful methane combustion and carbon removal trend than methane cracking at temperatures below 900°C. The details will be elaborated in the following section.

3.4. Promoting Catalytic Removal of Coke Deposit. Increasing the MgO component in the precursor enhances the tetragonal phase stability against reducing action of methane and syngas. The benefit of retaining the tetragonal phase lies in reserving oxygen vacancies (Figure 5) to assist the catalytic combustion of methane and removal of deposited surface carbon (Table 3). Noncatalytic methane combustion

happens at temperature as high as 1300°C, while an effective catalyst could lower the methane combustion temperature to as low as 400°C [40, 41]. It has been generally agreed that the POM mechanism involves two consecutive reactions, that is, methane combustion (2) followed by H₂O/CO₂ reforming ((3) and (4)).



The methane conversion is determined by the methane consumption rate through the reactions (2), (3), and (4). Under the present experimental condition (CH₄:O₂ = 2:1 and $T > 700^\circ\text{C}$), reaction (2) could rapidly reach its equilibrium and contribute to the methane conversion by up to nearly 25%. Therefore, reactions (3) and (4) contribute the main part of methane conversion. The reactions (3) and (4) proceed through the pyrolysis mechanism, in which the methane is first cracked on the metallic Ni⁰ particles as shown by step (5) to form coke [42]. The carbon species generated are subsequently removed via the reactions ((6) and (7)) with water and CO₂ produced from the combustion (2) [31, 43].



The C_s removal rate (R_{re}) is the summation of C_s removal rates of reactions (6) and (7). When the C_s removal rate (R_{re}) is greater than the pyrolysis rate or the carbon deposition rate (R_{cr}) (5), no filamentous carbon will be formed over the nickel catalyst surface. The catalyst with nil MgO doping permits prevalent pyrolysis owing to the presence of aggregated Ni⁰ particles (Figure 4(a)); hence, the coking was inevitable as proved by micrograph (Figure 11). On the contrary, with the increase in MgO doping extent, the number and sizes of Ni⁰ catalytic sites were reduced and some of them were shielded by La-Sr-O and MgO as pointed out above. This obviously led to reduction of the methane pyrolysis rate (the R_{cr} value). On the other hand, the tetragonal phase preserved during POM can contribute to the C_s removal (R_{re}) via supplying lattice oxygen. The methane conversion due to steam reforming (4) and dry reforming (3) is determined by whether R_{cr} or R_{re} is larger. In the low MgO doping extent range ($x < 0.2$), $R_{cr} > R_{re}$, the methane conversion increases as the doping of MgO rises, on the contrary, in the high MgO doping range ($x \geq 0.3$), $R_{cr} < R_{re}$, the methane conversion decreases as the doping of MgO rises. Consequently, the catalyst with MgO doping $x = 0.2$ realized a marginally greater R_{re} than R_{cr} , which prevents coking but also maintains the highest methane conversion and maximum CO and H₂ selectivity.

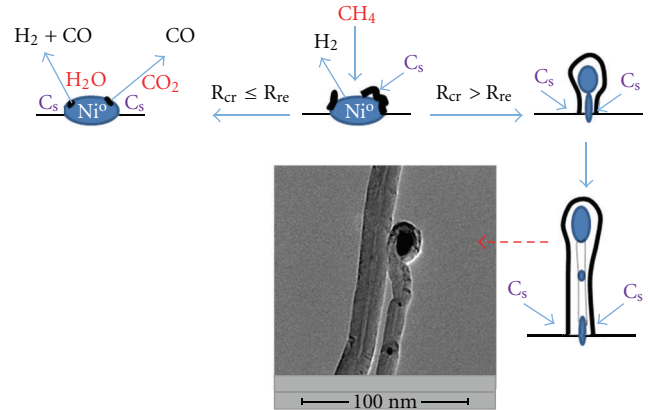


FIGURE 11: Schematic representation of the filamentous carbon fiber formation process during POM reaction.

4. Conclusions

This work started with the attempt of utilizing the solid state reaction equilibrium between the rock salt NiO-MgO solid solution and the tetragonal (La₂Sr_{1-z})₂Ni_yMg_{1-y}O_{3-δ} (LSNM) phase to reduce the size of NiO-MgO phase. This size reduction aimed to improve the coke resistance of the Ni⁰ catalyst in the partial oxidation of methane (POM) without compromising the activity of catalyst. A uniform oxide mixture 0.4 La₂O₃-0.2 SrCO₃-(1-x)NiO-xMgO, where $0 \leq x \leq 0.5$, was subjected to calcination at 800°C to establish the above solid solution equilibrium. The equilibrium shifts to the tetragonal phase side with the increasing of the stoichiometric coefficient x . The XRD characterization of the resulting oxide composites proved this shift of equilibrium. Furthermore, the chemical environments of nickel ions were scrutinized using temperature-programmed reduction (TPR). It showed that the LSMN becomes less reducible with increasing of the Mg²⁺ doping extent, similarly the rise of MgO content in the NiO-MgO phase lowers down the reducibility of it. The lattice oxygen vacancy concentration in LSMN was examined by means of temperature-programmed desorption and X-ray photoelectron spectroscopy. The above composites, when employed to catalyze the partial oxidation of methane, released two types of Ni⁰ sites as indicated by TPR: those embedded in the matrix of the reduced tetragonal phase and those embedded in MgO. The latter one was proven to be the main catalytic site as it existed as nanoparticles and more exposed relative to the former type. As a result, the methane conversion rate attained its climax with using the composite possessing stoichiometric coefficient $x = 0.2$ as the precursor of catalyst. On the contrary, the precursor with $x = 0$ turned out to be low reactive and heavily coke deposited on Ni particles. Increasing x level in this range boosted the dispersity of Ni clusters, which were also embedded in MgO matrix. However, the higher MgO contents ($x > 0.2$) led to decreasing of methane conversion rate. This outcome is attributed to a short of the Ni catalytic sites due to the reduction of the NiO-MgO phase with the increase in MgO dose used. The location of Ni clusters (in MgO) and the

decrease in reducibility of the tetragonal phase contribute to coke resistance of the catalyst. From viewpoint of POM mechanism, the reduction in Ni⁰ clusters lowers down the pyrolysis rate of methane on the clusters but raises the reforming rate of the coke generated.

Acknowledgment

The work has been performed with the financial support by NRF/CRP “Molecular engineering of membrane research and technology for energy development: hydrogen, natural gas, and syngas” (R-279-000-261-281).

References

- [1] L. Chen, Y. Lu, Q. Hong, J. Lin, and F. M. Dautzenberg, “Catalytic partial oxidation of methane to syngas over Ca-decorated-Al₂O₃-supported Ni and NiB catalysts,” *Applied Catalysis A*, vol. 292, no. 1-2, pp. 295–304, 2005.
- [2] H. Y. Wang and E. Ruckenstein, “CO₂ reforming of CH₄ over Co/MgO solid solution catalysts—effect of calcination temperature and Co loading,” *Applied Catalysis A: General*, vol. 209, pp. 207–215, 2001.
- [3] Y. H. Hu and E. Ruckenstein, “Binary MgO-based solid solution catalysts for methane conversion to syngas,” *Catalysis Reviews—Science and Engineering*, vol. 44, no. 3, pp. 423–453, 2002.
- [4] J. Requieres, M. A. Cabrero, V. L. Barrio et al., “Partial oxidation of methane to syngas over Ni/MgO and Ni/La₂O₃ catalysts,” *Applied Catalysis A*, vol. 289, no. 2, pp. 214–223, 2005.
- [5] J. R. Rostrup-Nielsen, “New aspects of syngas production and use,” *Catalysis Today*, vol. 63, no. 2–4, pp. 159–164, 2000.
- [6] J. Requieres, V. L. Barrio, J. F. Cambra et al., “Effect of redox additives over Ni/Al₂O₃ catalysts on syngas production via methane catalytic partial oxidation,” *Fuel*, vol. 87, no. 15-16, pp. 3223–3231, 2008.
- [7] T. Rostrup-Nielsen, “Manufacture of hydrogen,” *Catalysis Today*, vol. 106, no. 1–4, pp. 293–296, 2005.
- [8] S. Freni, G. Calogero, and S. Cavallaro, “Hydrogen production from methane through catalytic partial oxidation reactions,” *Journal of Power Sources*, vol. 87, no. 1, pp. 28–38, 2000.
- [9] Y. Mukainakano, K. Yoshida, S. Kado, K. Okumura, K. Kunimori, and K. Tomishige, “Catalytic performance and characterization of Pt-Ni bimetallic catalysts for oxidative steam reforming of methane,” *Chemical Engineering Science*, vol. 63, no. 20, pp. 4891–4901, 2008.
- [10] B. C. Enger, R. Lødeng, and A. Holmen, “A review of catalytic partial oxidation of methane to synthesis gas with emphasis on reaction mechanisms over transition metal catalysts,” *Applied Catalysis A*, vol. 346, no. 1-2, pp. 1–27, 2008.
- [11] V. R. Choudhary, K. C. Mondal, and T. V. Choudhary, “Partial oxidation of methane to syngas with or without simultaneous steam or CO₂ reforming over a high-temperature stable-NiCoMgCeO_x supported on zirconia-hafnia catalyst,” *Applied Catalysis A*, vol. 306, pp. 45–50, 2006.
- [12] Q. Miao, G. Xiong, S. Sheng, W. Cui, L. Xu, and X. Guo, “Partial oxidation of methane to syngas over nickel-based catalysts modified by alkali metal oxide and rare earth metal oxide,” *Applied Catalysis A*, vol. 154, no. 1-2, pp. 17–27, 1997.
- [13] J. H. Jun, T. J. Lee, T. H. Lim, S. W. Nam, S. A. Hong, and K. J. Yoon, “Nickel-calcium phosphate/hydroxyapatite catalysts for partial oxidation of methane to syngas: characterization and activation,” *Journal of Catalysis*, vol. 221, no. 1, pp. 178–190, 2004.
- [14] M. Prettre, C. Eichner, and M. Perrin, “The catalytic oxidation of methane to carbon monoxide and hydrogen,” *Transactions of the Faraday Society*, vol. 42, pp. 335–340, 1946.
- [15] S. Liu, G. Xiong, W. Yang, and S. Sheng, “The effect of Li and La on NiO/Al₂O₃ catalyst for CH₄/O₂ to syngas reaction,” *Reaction Kinetics and Catalysis Letters*, vol. 68, no. 2, pp. 243–247, 1999.
- [16] E. Ruckenstein and Y. H. Hu, “Methane partial oxidation over NiO/MgO solid solution catalysts,” *Applied Catalysis A*, vol. 183, no. 1, pp. 85–92, 1999.
- [17] S. L. González-Cortés, J. Orozco, D. Moronta, B. Fontal, and F. E. Imbert, “Methane conversion over Sr₂+/La₂O₃ catalyst modified with nickel and copper,” *Reaction Kinetics and Catalysis Letters*, vol. 69, no. 1, pp. 145–152, 2000.
- [18] L. Cao, Y. Chen, and W. Li, “Effect of La₂O₃ added to NiO/Al₂O₃ catalyst on partial oxidation of methane to syngas,” *Studies in Surface Science and Catalysis*, vol. 107, pp. 467–471, 1997.
- [19] V. R. Choudhary, K. C. Mondal, and A. S. Mamman, “High-temperature stable and highly active/selective supported NiCoMgCeO_x catalyst suitable for autothermal reforming of methane to syngas,” *Journal of Catalysis*, vol. 233, no. 1, pp. 36–40, 2005.
- [20] V. R. Choudhary, K. C. Mondal, and T. V. Choudhary, “Oxy-methane reforming over high temperature stable NiCoMgCeO_x and NiCoMgO_x supported on zirconia-hafnia catalysts: accelerated sulfur deactivation and regeneration,” *Catalysis Communications*, vol. 8, no. 3, pp. 561–564, 2007.
- [21] M. G. González, N. N. Nichio, B. Moraweck, and G. Martin, “Role of chromium in the stability of Ni/Al₂O₃ catalysts for natural gas reforming,” *Materials Letters*, vol. 45, no. 1, pp. 15–18, 2000.
- [22] R. Shiozaki, A. G. Andersen, T. Hayakawa et al., “Partial oxidation of methane over a Ni/BaTiO₃ catalyst prepared by solid phase crystallization,” *Journal of the Chemical Society—Faraday Transactions*, vol. 93, no. 17, pp. 3235–3242, 1997.
- [23] V. R. Choudhary, B. S. Uphade, and A. A. Belhekar, “Oxidative conversion of methane to syngas over LaNiO₃ perovskite with or without simultaneous steam and CO₂ reforming reactions: influence of partial substitution of La and Ni,” *Journal of Catalysis*, vol. 163, no. 2, pp. 312–318, 1996.
- [24] S. M. de Lima and J. M. Assaf, “Ni-Fe catalysts based on perovskite-type oxides for dry reforming of methane to syngas,” *Catalysis Letters*, vol. 108, no. 1-2, pp. 63–70, 2006.
- [25] R. Shiozaki, A. G. Andersen, T. Hayakawa et al., “Sustainable Ni/BaTiO₃ Catalysts for Partial Oxidation of Methane to Synthesis Gas,” *Studies in Surface Science and Catalysis*, vol. 111, pp. 701–710, 1997.
- [26] R. N. Basu, F. Tietz, E. Wessel, H. P. Buchkremer, and D. Stöver, “Microstructure and electrical conductivity of LaNi_{0.6}Fe_{0.4}O₃ prepared by combustion synthesis routes,” *Materials Research Bulletin*, vol. 39, no. 9, pp. 1335–1345, 2004.
- [27] H. Provendier, C. Petit, C. Estournès, S. Libs, and A. Kienemann, “Stabilisation of active nickel catalysts in partial oxidation of methane to synthesis gas by iron addition,” *Applied Catalysis A*, vol. 180, no. 1-2, pp. 163–173, 1999.
- [28] E. V. Tsipis, E. A. Kiselev, V. A. Kolotygin, J. C. Waerenborgh, V. A. Cherepanov, and V. V. Kharton, “Mixed conductivity, Mössbauer spectra and thermal expansion of (La,Sr)(Fe,Ni)O₃— δ perovskites,” *Solid State Ionics*, vol. 179, no. 38, pp. 2170–2180, 2008.

- [29] S. Takenaka, H. Umebayashi, E. Tanabe, H. Matsune, and M. Kishida, "Specific performance of silica-coated Ni catalysts for the partial oxidation of methane to synthesis gas," *Journal of Catalysis*, vol. 245, no. 2, pp. 392–400, 2007.
- [30] A. Iriondo, M. B. Güemez, V. L. Barrio et al., "Glycerol conversion into H₂ by steam reforming over Ni and PtNi catalysts supported on MgO modified γ -Al₂O₃," *Studies in Surface Science and Catalysis*, vol. 175, pp. 449–452, 2010.
- [31] X. Yin and L. Hong, "Partial oxidation of methane to syngas over the catalyst derived from double perovskite (La_{0.5}Sr_{0.5})₂FeNiO_{6- δ} ," *Applied Catalysis A*, vol. 371, no. 1-2, pp. 153–160, 2009.
- [32] H. J. Wei, Y. Cao, W. J. Ji, and C. T. Au, "Lattice oxygen of La_{1-x}Sr_xMO₃ (M = Mn, Ni) and LaMnO_{3- α} F _{β} perovskite oxides for the partial oxidation of methane to synthesis gas," *Catalysis Communications*, vol. 9, no. 15, pp. 2509–2514, 2008.
- [33] G. S. Gallego, F. Mondragón, J. Barrault, J. M. Tatibouët, and C. Batiot-Dupeyrat, "CO₂ reforming of CH₄ over La-Ni based perovskite precursors," *Applied Catalysis A*, vol. 311, no. 1-2, pp. 164–171, 2006.
- [34] S. N. Pavlova, N. N. Sazonova, V. A. Sadykov et al., "Selective catalytic oxidation of methane to syngas over supported mixed oxides containing Ni and Pt," *Kinetics and Catalysis*, vol. 45, no. 4, pp. 589–597, 2004.
- [35] J. Zhu, X. Yang, X. Xu, and K. Wei, "Effect of strontium substitution on the activity of La_{2-x}Sr_xNiO₄ (x = 0.0–1.2) in NO decomposition," *Science in China, Series B*, vol. 50, no. 1, pp. 41–46, 2007.
- [36] N. Li, A. Boréave, J. P. Deloume, and F. Gaillard, "Catalytic combustion of toluene over a Sr and Fe substituted LaCoO₃ perovskite," *Solid State Ionics*, vol. 179, no. 27–32, pp. 1396–1400, 2008.
- [37] A. Yan, B. Liu, Y. Dong, Z. Tian, D. Wang, and M. Cheng, "A temperature programmed desorption investigation on the interaction of Ba_{0.5}Sr_{0.5}Co_{0.8}Fe_{0.2}O_{3- δ} perovskite oxides with CO₂ in the absence and presence of H₂O and O₂," *Applied Catalysis B*, vol. 80, no. 1-2, pp. 24–31, 2008.
- [38] S. Royer, D. Duprez, and S. Kaliaguine, "Oxygen mobility in LaCoO₃ perovskites," *Catalysis Today*, vol. 112, no. 1–4, pp. 99–102, 2006.
- [39] M. R. Goldwasser, M. E. Rivas, E. Pietri et al., "Perovskites as catalysts precursors: synthesis and characterization," *Journal of Molecular Catalysis A*, vol. 228, no. 1-2, pp. 325–331, 2005.
- [40] J. G. McCarty, "Durable catalysts for cleaner air," *Nature*, vol. 403, no. 6765, pp. 35–36, 2000.
- [41] A. J. Zarur and J. V. Ying, "Reverse microemulsion synthesis of nanostructured complex oxides for catalytic combustion," *Nature*, vol. 403, no. 6765, pp. 65–67, 2000.
- [42] E. P. Murray, T. Tsai, and S. A. Barnett, "A direct-methane fuel cell with a ceria-based anode," *Nature*, vol. 400, no. 6745, pp. 649–651, 1999.
- [43] X. Yin, L. Hong, and Z. L. Liu, "Asymmetric tubular oxygen-permeable ceramic membrane reactor for partial oxidation of methane," *Journal of Physical Chemistry C*, vol. 111, no. 26, pp. 9194–9202, 2007.



Hindawi

Submit your manuscripts at
<http://www.hindawi.com>

